Evidence of strong correlations at the van Hove singularity in the scanning tunneling spectra of superconducting Bi_{2}Sr_{2}CaCu_{2}O_{8+δ} single crystals

Jouko Nieminen, Ilpo Suominen, Tanmoy Das, R. S. Markiewicz, and A. Bansil

Phys. Rev. B **85**, 214504 — Published 4 June 2012

DOI: 10.1103/PhysRevB.85.214504

Model evidence of strong correlations at the van Hove singularity in the scanning-tunneling spectra of superconducting $Bi_2Sr_2CaCu_2O_{8+\delta}$ single crystals

Jouko Nieminen*
Department of Physics, Tampere University of Technology, P.O. Box 692, FIN-33101 Tampere, Finland and Department of Physics, Northeastern University, Boston

Ilpo Suominen
Department of Physics, Tampere University of Technology, P.O. Box 692, FIN-33101 Tampere, Finland

Tanmoy Das, R.S. Markiewicz, and A. Bansil
Department of Physics, Northeastern University, Boston
(Dated: Version of May 14, 2012)

We present realistic multiband calculations of scanning tunneling spectra in $Bi_2Sr_2CaCu_2O_{8+\delta}$ over a wide doping range. Our modeling incorporates effects of a competing pseudogap and pairing gap as well as effects of strong electronic correlations, which are included by introducing self-energy corrections in the one-particle propagators. The calculations provide a good description of the two-gap features seen in experiments at low energies and the evolution of the Van Hove singularity (VHS) with doping, and suggest a possible quantum critical point near the point where the VHS crosses the Fermi level.

PACS numbers: 68.37.Ef 74.50.+r 74.20.Pq 74.72.Gh

I. INTRODUCTION

A curious, topological feature of any two dimensional electronic band is a saddle-point Van Hove singularity (VHS), which can lead to a crossover from electron-like to hole like Fermi surfaces with doping, accompanied by a logarithmically diverging density-of-states (DOS) and a vanishing Fermi velocity[1]. While the divergence itself can easily be smoothened by disorder or interlayer coupling, the presence of a peak in the DOS is a robust feature of the underlying spectrum. In hole-doped cuprates, most theoretical studies of doping dependence find enhanced tendencies for superconductivity or competing phases – including the possibility of phase separation – when this VHS approaches the Fermi level E_F.[2,3] This scenario seems to work for $La_{2-x}Sr_xCuO_4$, where the VHS nearly coincides with E_F at optimal doping[4], but in most other cuprates, with a larger second-neighbor hopping parameter t', optimal doping and the VHS doping seem to separate further as T_c increases.[5] Notably, early angle-resolved photoemission spectroscopy (ARPES) experiments found evidence for a peak-dip-hump structure, where an electronic mode pushed a narrow coherent band with a prominent VHS ('peak') very close to the Fermi level of most cuprates, while pushing incoherent spectral weight away from E_F ('hump'), thereby leaving a 'dip' in the spectrum near the mode energy.[6] However, the coherent VHS peak has proved elusive in these materials, and there is controversy as to whether it can be seen in tunneling spectroscopy[7,8].

Here we explore this issue by comparing recent scanning tunneling microscopy and spectroscopy (STM/STS) data with a realistic multiband modeling of the spectra in $Bi_2Sr_2CaCu_2O_{8+\delta}$ (Bi-2212). The model is able to reproduce the STM features in detail, shedding light on the role of the VHS and the ordering phenomena involved in 'two gap' physics.

Our doping-dependent tunneling spectrum is calculated using a multiband Nambu-Gorkov Green's function tensor formalism. The main technical innovation of this work is to incorporate a variety of intermediate coupling effects into the tunneling formalism via a tensor self-energy extracted from quasiparticle-GW (QP-GW) calculations.[9]. We model the two competing order gaps as due to BCS-type SC coupling[10,11] and antiferromagnetic order. To these we add intermediate coupling self-energies, calculated in a GW model. Our QP-GW self-energies have been shown to capture a wide range of phenomena in cuprates over an extended range of doping and excitation energies, including the relationship between magnetic order and superconductivity, and the so-called waterfall physics.[12] Notably, for a realistic consideration of the features in STM/STS, it is essential to utilize a multiband framework. This makes it possible to incorporate filtering and tunneling path effects due to the BiO and SrO layers separating the vacuum and the cuprate layers, and the important role of the apical oxygen and Cu d_{z^2} orbitals.[10,11]

While the one band QP-GW model employed to obtain the self-energies used in this study is nearly parameter-free[13], the present calculations unavoidably introduce additional parameters due to two separate factors. Firstly, the pairing gaps are treated as parameters, since the Eliashberg theory cannot accurately predict the gap size, particularly in the pseudogap phase. A second set of parameters arises because STM experiments on the cuprates find that the gap size varies in different local patches across a given crystal. In our modeling, we as-

sume that different patches represent regions of different local doping[14–18]. A strong inference from our study is support for this local doping model since a number of observed spectral features can be correlated with theory over a wide range of energies and dopings.

This article is organized as follows. Section II describes our model of electronic spectrum and gives a brief overview of the formalism of tunneling calculations. Section III presents theoretical results for the normal and the superconducting state as a function of doping and compares and contrasts these results with the corresponding experimental results, including issues related to the two-gap physics and signatures of the VHS. Section IV discusses broader implications of our study. This is followed by a summary of our conclusions in Section V. Appendix A gives details of the interaction terms used in the Hamiltonian, while Appendix B discusses details of the self-energy corrections used for incorporating electron correlation effects in our tunneling computations. Appendix C summarizes a related model which displays peak-dip-hump physics.

II. METHODOLOGY

A. Green's function formulation of tunneling current

Our computations are based on a multiband tight-binding model using 4×116 orbitals per unit cell, i.e., a fourfold basis taking into account electrons and holes for both spin directions.[10,11] For treating the magnetic order and superconducting pairing, the tensor (Nambu-Gorkov) Green's function $\mathcal{G}$ is employed with the corresponding Dyson's equation:[19]

$$\mathcal{G} = \mathcal{G}^0 + \mathcal{G}\mathcal{V}\mathcal{G}^0, \tag{1}$$

where

$$\mathcal{G} = \begin{pmatrix} G_{e\uparrow} & 0 & 0 & F_{\uparrow\downarrow} \\ 0 & G_{e\downarrow} & F_{\downarrow\uparrow} & 0 \\ 0 & F^\dagger_{\downarrow\uparrow} & G_{h\uparrow} & 0 \\ F^\dagger_{\uparrow\downarrow} & 0 & 0 & G_{h\downarrow} \end{pmatrix} \text{ with } c_\alpha = \begin{pmatrix} c_{\alpha\uparrow} \\ c_{\alpha\downarrow} \\ c^\dagger_{\alpha\uparrow} \\ c^\dagger_{\alpha\downarrow} \end{pmatrix}$$

where G_e and G_h, denote the Green's functions for the electrons and holes, respectively[20], and the matrix elements of operator $\mathcal{V}$ represent the interaction terms of Hamiltonian of Eq. (7), below.

In the tunneling calculations the filtering effect of the surface layers is taken into account by using the Todorov-Pendry approach[21] in which the differential conductance σ between orbitals of the tip (t, t') and the sample (s, s') is given by[10,11]

$$\sigma = \frac{dI}{dV} = \frac{2\pi e^2}{\hbar} \sum_{tt's s'} \rho_{tt'}(E_F) V_{t's} \rho_{ss'}(E_F + eV) V^\dagger_{s't}, \tag{2}$$

where the density matrix

$$\rho_{ss'} = -\frac{1}{\pi} Im[G^+_{ss'}] = \frac{1}{2\pi i}\left(G^-_{ss'} - G^+_{ss'}\right), \tag{3}$$

is expressed in terms of the retarded and advanced electron Green function or propagators. Eq. 2 differs from the more commonly used Tersoff-Hamann formulation[22] in that it takes into account the details of the symmetry of the tip orbitals and how these orbitals couple with the orbitals of the cuprate layer through the filtering BiO and SrO layers.

Equation 3 can be rewritten as[11]

$$\sigma = \frac{2\pi e^2}{\hbar} \sum_{tt'cc'} \rho_{tt'}(E_F) M_{t'c} \rho_{cc'}(E_F + eV) M^\dagger_{c't}, \tag{4}$$

where

$$M_{tc} = V_{ts} G^{0+}_{sf} V_{fc}, \tag{5}$$

gives the filtering amplitude between the cuprate layer and the tip, and constitutes a multiband generalization of the filtering function of Ref. 23. Note that the matrix element of the density of states operator $\rho_{cc'}$ within the cuprate plane can be recovered in terms of the spectral function:

$$\rho_{cc'} = -\frac{1}{\pi} \sum_\alpha (G^+_{c\alpha} \Sigma''_\alpha G^-_{\alpha c'} + F^+_{c\alpha} \Sigma''_\alpha F^-_{\alpha c'}) \tag{6}$$

Notably, the matrix M itself is rather structureless, but it is very selective in the way it couples the insulating layers and the cuprate layer due to the term V_{fc}.[11] In fact, for symmetry reasons the tunneling channel passes through the d_{z^2} orbital and not the $d_{x^2-y^2}$ orbital of the Cu atoms.

B. Interaction Effects

In order to meaningfully describe the doping dependence of the tunneling spectra of the cuprates, various key interactions must be included in the Hamiltonian. To this end, we introduce interactions via a Hubbard U on the Cu sites, which are approximated by a mean-field antiferromagnetic order plus GW-type self-energy associated with spin and charge fluctuations. We model the two competing order gaps as being due to a BCS-type SC coupling, and an antiferromagnetic order. Superconductivity is included by adding a d-wave pairing interaction term Δ and the AFM order[24] is included by introducing a Hubbard term Um, leading to the Hamiltonian:

$$\begin{aligned} \hat{H} = \textstyle\sum_{\alpha\beta\sigma}(\varepsilon_\alpha c^\dagger_{\alpha\sigma} c_{\alpha\sigma} + V_{\alpha\beta} c^\dagger_{\alpha\sigma} c_{\beta\sigma} + \Delta_{\alpha\beta} c^\dagger_{\alpha\sigma} c^\dagger_{\beta-\sigma} + \\ \Delta^\dagger_{\beta\alpha} c_{\beta-\sigma} c_{\alpha\sigma}) - \textstyle\sum_\alpha U m_\alpha (c^\dagger_{\alpha\uparrow} c_{\alpha\uparrow} - c^\dagger_{\alpha\downarrow} c_{\alpha\downarrow}) \end{aligned} \tag{7}$$

with the real-space creation (annihilation) operators $c^\dagger_{\alpha\sigma}$ ($c_{\alpha\sigma}$). Here α is a composite index for the type of orbital

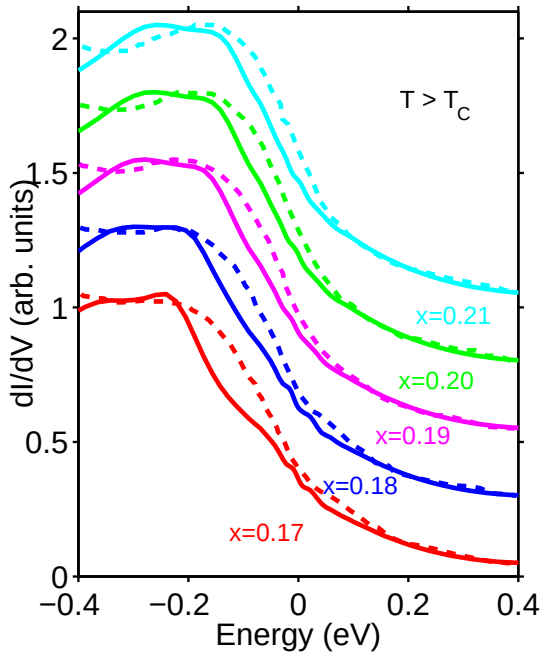

FIG. 1: (Color online) Comparison of the theoretical (solid) and experimental (dashed, Ref. 28) normal state STS spectra over the hole doping range $x = 0.21 - 0.17$.

and its site, and σ is the spin index. ε_α is the on-site orbital energy, while $V_{\alpha\beta}$ is the hopping integral between orbitals α and β.[25–27] The band structure related parameters ε_α and $V_{\alpha\beta}$ are the same as those used in Ref. 11. Details of the interaction parameters U, m, and Δ are given in Appendix A.

In order to model effects of the low and high energy bosonic couplings and background scattering in the electronic system, we add a self-energy correction in the propagators, which consists of three distinct contributions:

$$\Sigma_{\alpha\beta}(\varepsilon) = \Sigma^L_{\alpha\beta}(\varepsilon) + \Sigma^H_{\alpha\beta}(\varepsilon) + \Sigma^{imp}_{\alpha\beta}(\varepsilon). \qquad (8)$$

Here, superscripts L and H refer to corrections due to the low- and high-energy bosonic couplings, respectively, while the superscript *imp* refers to the correction term arising from background impurity scattering. For Σ^L we use a phonon contribution based on a Debye spectrum and Σ^H is obtained within the framework of a self-consistent GW scheme. Details of the self-energy corrections of Eq. 8, including an overview of the GW-scheme used, are given in Appendix B. We note that in the theoretical STS spectra discussed in Section III below, the electronic contribution Σ^H dominates in producing key features in the spectra, while Σ^{imp} yields a realistic broadening of the spectra and Σ^L contributes to the sharpness of the coherence peaks.

III. RESULTS

A. Normal State Spectra

Fig. 1 compares the normal state spectra taken above the superconducting transition temperature T_c where superconductivity is absent although a pseudogap could be present. Experimental data over a wide energy range are available only near and above optimal doping where the pseudogap is small or zero.[28] In Ref. 28, the superconducting gap map of an inhomogenous sample was first measured at low temperature to determine the local gap Δ in different domains on the surface. The temperature was then raised above the highest superconducting transition temperature, and the corresponding normal state spectra were measured. Along these lines[14,15], we use the measured low-T gap values varying from 20 meV to 36 meV to adduce the local doping, which yields doping values varying over $x = 0.21 - 0.17$ as shown in Fig. 1. The theoretical as well as the experimental spectra in Fig. 1 are seen to be quite featureless, except for the pronounced asymmetry between high positive and negative bias voltages, which we have analyzed previously.[10] The most prominent feature in the spectra is a large hump-like feature located around -200 meV binding energy for x= 0.21, which shifts away from the Fermi level to higher binding energies and becomes smoother as the doping is decreased. Our calculations are seen to reproduce this hump-like feature and its characteristic shift and smoothening with doping in substantial accord with experimental results. It should be noted that over the doping range considered in Fig. 1, pseudogap effects in our computations are quite small. We have verified this by carrying out a series of computations where the pseudogap was artificially turned off (not shown in Fig. 1 for brevity), suggesting that the pseudogaps have closed at the temperature of 93K at which the experimental data are taken.

Figure 2(a) gives a plot of the energies of various features in the theoretical and experimental STS spectra of Fig. 1 to allow a more quantitative discussion of the doping dependencies of these features and their correlation with the phase diagram of Bi2212. The model includes bilayer splitting, and the solid blue [short-dashed red] curve represents the VHS peak of the antibonding [bonding] band. We see that the experimental normal state hump (blue filled circles)[28] is in good agreement with the doping dependence of the antibonding VHS. The calculated VHS position does not change significantly in the superconducting state, so we also plot the experimental hump feature from the superconducting state (violet filled diamonds)[17], from Fig. 3 below. When an AF pseudogap turns on, a second feature appears [green long-dashed and orange dotted lines for the antibonding and bonding bands respectively]. Frames (b) and (c) explain the origin of this feature for the antibonding band, labeled B. These figures are based on a three-band model, containing a Cu $d_{x^2-y^2}$ and two O p orbitals, in which

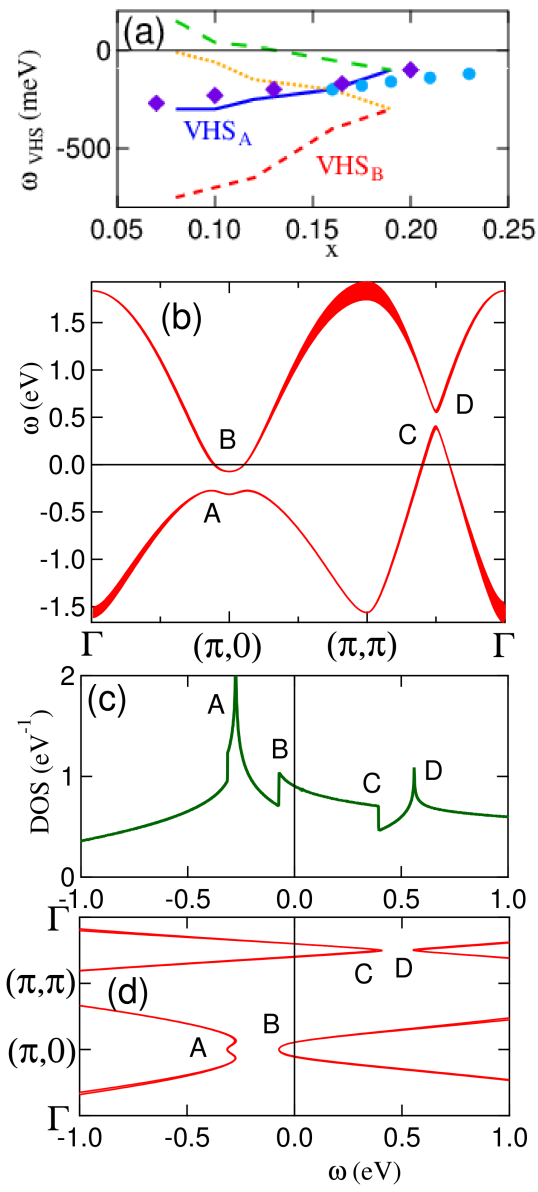

FIG. 2: (Color online) (a) Derived AF state phase diagram. The filled blue circles [Ref. 28] and violet diamonds [Ref. 17] are the hump features for Bi2212 derived from recent STM measurements. These are compared to a calculated doping dependence of the bonding [B] and antibonding [A] VHS (red short-dashed and blue solid lines, respectively) in Bi2212, based on the present analysis. (b) Calculated dispersion at $x = 0.15$, with feature A, the VHS of the lower magnetic band, corresponding to the blue solid line [or red short-dashed line, for the bonding band] in (a), and feature B, the bottom of the upper magnetic band, corresponding to the green long-dashed line [orange dotted line] in (a). The thickness of the lines represents the spectral weight due to the AF structure factor. (c) Corresponding DOS, showing features derived from A, B, C, and D in (b). (d) Blow-up of the near-E_F dispersion.

bilayer splitting is neglected, to clarify the origin of the features. From Fig. 3(b), it can be seen that the AF gap has a strong k-dependence, splitting the band into upper and lower magnetic bands (U/LMBs). Features A and D are the VHSs of the LMB and UMB respectively, while feature B is the bottom of the UMB and feature C the top of the LMB. Note the characteristic form of the DOS associated with each feature in Fig. 2(c).

As the AF pseudogap shrinks to zero, features A and B [and C and D] merge. That is why there is no near-E_F feature in the three spectra in Fig. 1 with higher dopings. For lower doping a feature corresponding to B appears in the low-T theoretical curves, but seems to be absent in the T=93K experimental data of Fig. 1, suggesting a T-dependent pseudogap closing. Note that at lower doping feature B moves closer to the Fermi level, and should persist to higher temperatures, as the pseudogap is larger.

B. Superconducting State spectra

Figure 3(a) compares our theoretical results[29] with the corresponding experimental spectra[17,30] at five representative values of hole doping, with doping decreasing from the optimally doped SC phase at $x = 0.19$ at the top to the underdoped pseudogap phase for $x = 0.08$ at the bottom of the figure. With reference to Fig. 1, we see that the hump-like feature at negative energies and its characteristic doping dependency in the normal state is present also in the superconducting state spectra of Fig. 3 (plotted in Fig. 2(a)). The main difference between the normal and superconducting state spectra is the opening up of a complex gap structure at low energies, which is highlighted in the expanded view of Fig. 3(b).[31] We note here with reference to the lowest set of curves in Fig. 3(a) as an example that the STM spectra resemble the antinodal ARPES spectra.[32] Moreover, the angle-dependence of the gap function adduced from the STM quasiparticle interference maps is in good agreement with the gaps obtained via ARPES measurements.[33] These results support our use of the local gap to determine the local doping of the patches in STM data.

Figure 4 gives a plot of the two low-energy gaps from the theoretical STS spectra of Fig. 3, shown as filled and empty blue diamonds. These are seen to be in good agreement with the 'two gap' features extracted from ARPES[34,35] and with Raman results[36,37] for $HgBa_2CuO_{4+\delta}$ (Hg1201). The remaining curves[38,39] will be discussed below. Interestingly, our computations reproduce the remarkable *anticorrelation* displayed by the large hump feature at negative energies in the experimental STS spectra in Figs. 2 and 3 in the way it varies with doping in relation to the doping dependence of the size of the gap[28]. Specifically, with increasing doping, as the hump moves closer to the Fermi energy and the density of states at the Fermi energy increases, the size of the gap in Figs. 3 and 4 does not become larger as we

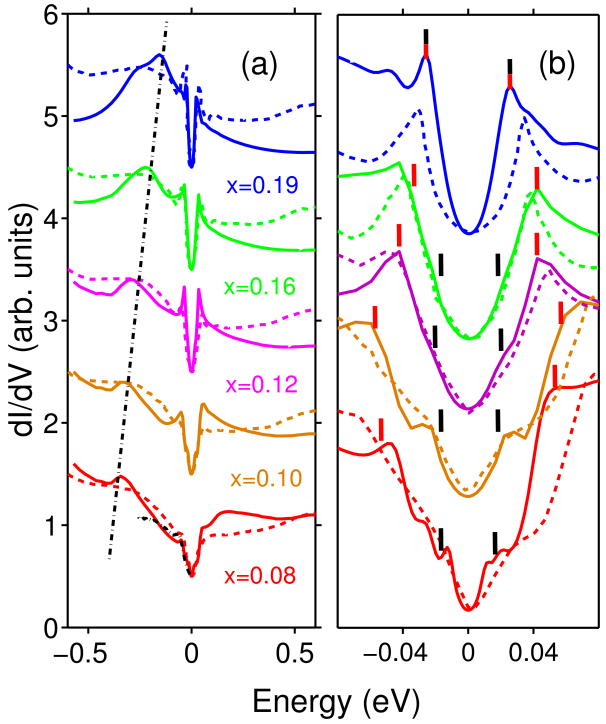

FIG. 3: (Color online) (a) Theoretical (solid) and experimental (dashed, Ref. 17) superconducting state spectra over the hole doping range from $x = 0.19$ at the top to $x = 0.08$ at the bottom of the figure.[29] For comparison, the experimental ARPES spectrum[32] at $x = 0.08$ (black dashed curve) is shown. The dot-dashed line is drawn through the hump feature in the computed spectra as a to guide the eye. (b) Blowup of theoretical spectra near the Fermi level is compared with the corresponding data of Ref. 30. The black and red bars indicate the gap widths shown as empty and filled diamonds in Fig. 4.

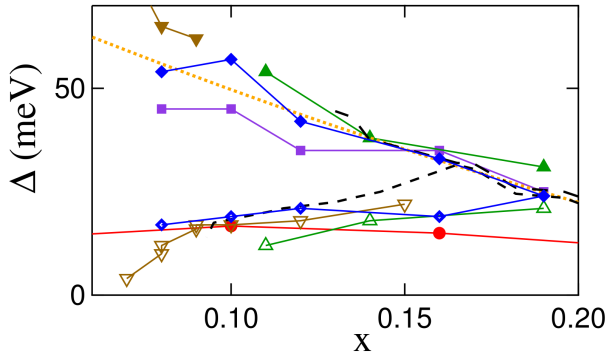

FIG. 4: (Color online) Two gap physics in the superconducting state. The two theoretical gaps from Fig. 3(b) are plotted as filled and empty blue diamonds and compared to experimental ARPES results from Ref. 34 (green triangles) and Ref. 35 (brown inverted triangles) and corresponding Raman results for $HgBa_2CuO_{4+\delta}$ (Hg1201) (black long- and short-dashed lines) from Ref. 37. Shown also is the input SC gap parameter, violet squares, the expected position of a VHS, based on an experimental ARPES dispersion[38], orange dotted line, and a calculated SC gap[39], red circles, to illustrate the doping dependence expected for a spin-pairing mechanism.

would expect from the BCS theory, but instead the gap becomes smaller. The size of the coherence peaks, on the other hand, is seen to grow with increasing doping in our theory in accord with experiments.

Fig. 5 gives insight into the origin of the two gap physics in Bi2212. For this purpose panel (a) gives a map of the spectral weight obtained from the imaginary part of the one-particle Green's function along the $\Gamma - X(\pi, 0) - M(\pi, \pi) - \Gamma$ line in the k-space. This map may be thought of as an effective theoretical E vs k spectrum resulting after the self-energy correction Σ has been applied to the propagators. In the absence of self-energy corrections, this map will consist of δ-function peaks arising from the real poles of the Green's function corresponding to the familiar energy bands of Bi2212 modified by the the AFM and SC orders.[40,41] At the doping of $x = 0.08$ considered in Fig. 5, the antibonding VHS lies around -300 meV, well below the Fermi energy. After self-energy corrections are introduced, the VHS is broadened substantially and yields the large hump-like structure in the local density of states around -300 meV as seen from the LDOS plot of Fig. 5(b) [leftmost arrow]. Due to bilayer splitting[42–46], the bonding VHS lies near -800 meV at this doping, and is not seen in Fig. 5.

Next, we address the features near E_F in Figs. 3(b) and 4 and how these features relate to the two-gap physics, which has been discussed in connection with Raman scattering[36,37], angle-resolved photoemission (ARPES)[34,35], and recent STM studies[47,48]. Two different components of the gap have been observed with different doping dependences[49]: a nodal pairing gap Δ_n with a parabolic doping dependence reminiscent of the superconducting T_c, and an antinodal gap Δ^* which increases roughly linearly with underdoping, similar to the pseudogap onset temperature T^*. The experimental near-gap features[30] in Figs. 3(b) and 4 clearly reflect the presence of two gaps, which are well captured by the present calculations. While the overdoped sample displays a single gap feature, samples at lower doping show four features comprising two gaps, an outer gap which grows with underdoping and an inner gap which shrinks (see Fig. 4), in good agreement with the two-gap scenario. Coherence peaks are prominent in the overdoped sample, but gradually disappear as doping is lowered, in good accord with the computed STM spectra. [In the undoped case we find a large magnetic gap, with no evidence of superconductivity (not shown).] From Fig. 3(b) it can be seen that our modeling reproduces the electron-hole asymmetry of the experimental coherence peaks, which is unexpected in the BCS formalism[50].

Fig. 6 gives the decomposition of the LDOS of Fig. 5(b) for x=0.08 into the spin-resolved contributions from

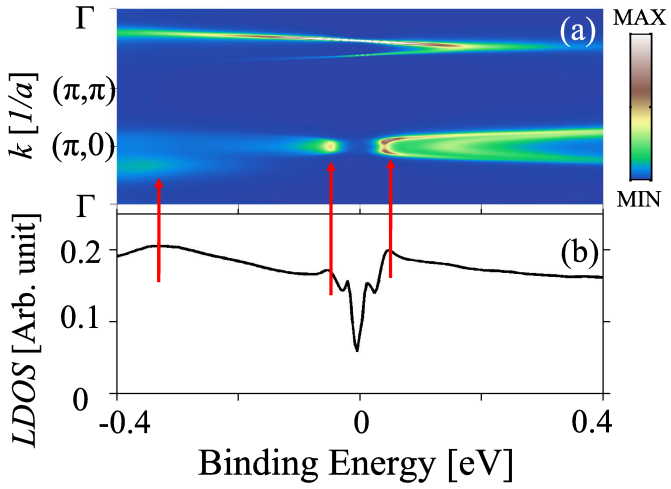

FIG. 5: (Color online) (a) Calculated $E-k$ spectral weight diagram for $x=0.08$ along high symmetry line $\Gamma-(\pi,\pi)-(\pi,0)-\Gamma$ in momentum space. White/brown color denotes high and blue color low intensity. (b) The corresponding total LDOS from Cu sites, with arrows relating three prominent LDOS peaks to spectral features in (a). Note that several peaks seen in LDOS in the low energy region do not show up in (a) because the associated spectral weight lies along the zone diagonal, which is not shown in (a) [see Fig. 6(b)].

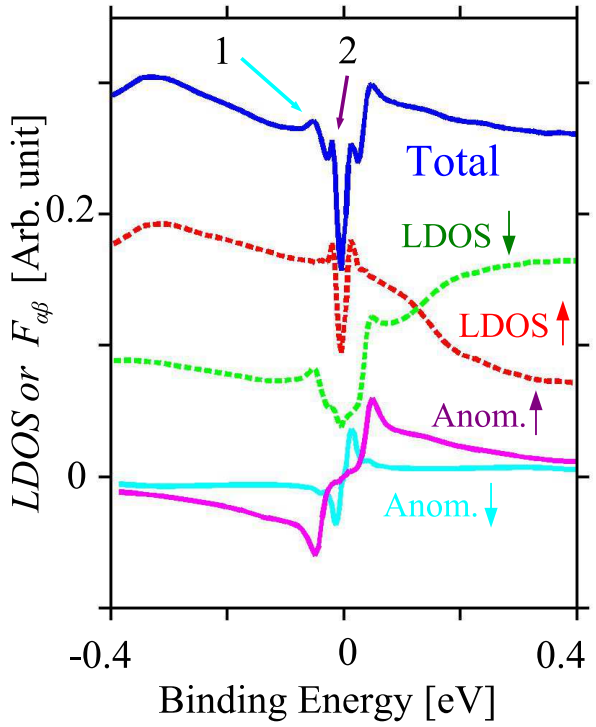

FIG. 6: (Color online) Calculated spin resolved LDOS of the Cu-d_{x2-y2} orbital for $x=0.08$: Total LDOS (blue solid line) and its decomposition into contributions from the lower magnetic band (LMB, red dashed line) and the upper magnetic band (UMB, green dashed line). Also shown are the corresponding imaginary parts (cyan and magenta solid lines) of the anomalous matrix elements $F_{\alpha\beta}$ of the Nambu-Gorkov Green's function for the d_{x2-y2} orbitals on two neighbouring Cu atoms. This matrix element indicates strong electron-hole hybridization or pairing effect at the pseudogap edge labeled by '1' and the in-gap peak labeled by '2' in the total LDOS (solid blue line).

the upper and lower magnetic bands (UMB and LMB). In our computations there is a small magnetic gap separating the UMB and LMB, leading to electron pockets near $(\pi,0)$ and hole pockets near $(\frac{\pi}{2},\frac{\pi}{2})$. The two gaps in the total LDOS curve in Fig. 6 are identified by the arrows labeled 1 and 2, and are plotted in Fig. 4 as blue diamonds. In order to clarify the role of pairing in these two features, Fig. 6 also shows the anomalous matrix elements $F_{\alpha\beta}$ of the Nambu-Gorkov Green's function[51], which can be used to monitor the pairing effect. The contribution of the anomalous elements to both the in-gap and gap-edge peaks indicates that pairing is involved in both features. Notably, the gap features in Fig. 3(b) more closely resemble the UMB features in Fig. 6, indicating that the tunneling matrix element couples differently to the LMB and UMB states.

Further insight into pairing can be obtained by considering the evolution of dispersions with binding energy. Fig. 7 shows spectral maps in momentum space at the energies of the coherence peaks for the lower edge of the pseudogap in frame (a) and for the lower in-gap peak in frame (b). The corresponding anomalous spectral weights are shown in frames (c) and (d). The peak at the pseudogap edge is associated with the top of the $(\pi,0)$ pocket as can be seen from the strong pairing intensity in Fig. 7(c). The in-gap peak is associated with the pairing gap on the $(\pi/2,\pi/2)$ pocket, Fig. 6(d), where AF order is absent. Note that at this energy the $(\pi,0)$ pocket is absent, Fig. 7(b). The $(\pi,0)$ peak is found to predominantly represent AF order with a Bilbro-McMillan-like dressing by superconductivity[52], while the $(\pi/2,\pi/2)$ peak is a pure SC gap. Note in Fig. 7(b) that the spectral weight of the $(\pi/2,\pi/2)$ pocket resembles an arc with peak intensity at the AF zone boundary as seen in STM studies. With decreasing doping the gap between the LMB and UMB increases, leading to a monotonically increasing pseudogap energy. In contrast, the Fermi surface on the LMB near $(\pi/2,\pi/2)$ shrinks monotonically since its area is proportional to x. For a d-wave gap which vanishes at $(\pi/2,\pi/2)$, its maximum value must ultimately decrease with underdoping, thereby explaining the opposite doping dependence of the two gaps.

C. Comparison with Bi2201

To gain more insight into the relation of E_{VHS} and the superconducting gap Δ, in Fig. 8 we compare the present results with recent experiments on $Bi_2Sr_2CuO_{6+\delta}$

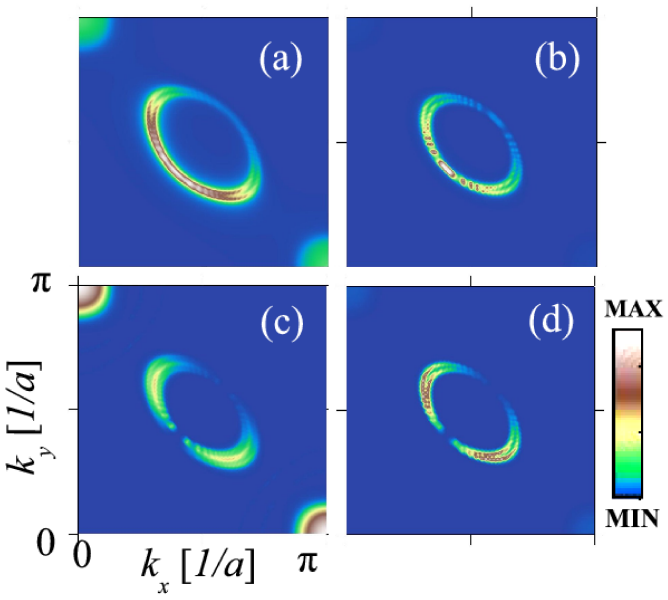

FIG. 7: (Color online) (a) Spectral map at constant energy for $x = 0.08$ for the regular matrix elements of the Nambu-Gorkov Green's function. The energy corresponds to the lower edge of the pseudogap, i.e. the energy of the peak marked 1 in Fig. 5. (b) Same as (a), except the energy corresponds to the energy of peak 2 in Fig. 5. (c) Same as (a), except it gives the spectral map for anomalous matrix elements of the Green's function at the energy of peak 1. (d) Same as (c) for the peak 2. Arcs in (c) and (d) have zero weight along the nodal line, where the gap vanishes.

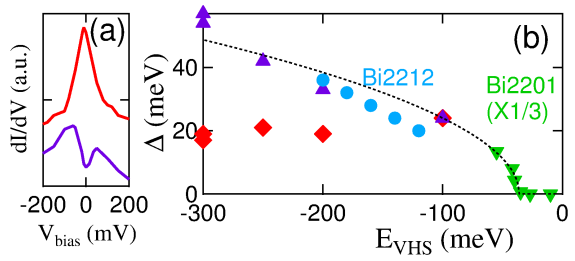

FIG. 8: (Color online) (a) Tunneling dI/dV spectra for Bi2201 corresponding to E_{VHS} = -10 meV (upper, red line) and -56 meV (lower, violet line, offset for clarity), after Ref. 8. (b) Plots of Δ vs E_{VHS} for Bi2212 (red diamonds and violet triangles from Ref. 30 and blue circles from Ref. 28) and Bi2201 (inverted green triangles from Ref. 8). Dotted line indicates a square-root dependence of Δ on $E_{VHS} + 36$ meV.

(Bi2201).[8] We see that the shape of the VHS at highest doping is consistent with the calculated shape in Bi2212 at lower doping compare the top curves in Fig. 3(a) and Fig. 8(a) but that it gets considerably broadened for slightly lower doping, lower curve in Fig. 8(a). This may explain why our calculations in Fig. 3(a) underestimate the VHS broadening, as the QP-GW technique tends to produce too little broadening at higher energies.

The decrease of Δ with increasing E_{VHS}, Fig. 8(b), is quite similar in both materials, although with somewhat faster change in Bi2201 (note change of scale). The remarkable resemblance to the dotted curve is unexpected, and deserves some comment. The dotted curve represents the relation

$$\Delta^2 + \Delta_0^2 = A|E_{VHS}|, \tag{9}$$

with $\Delta_0 \sim 18\ meV$, and $A \sim \Delta_0/2$. The general form $\sum_i \Delta_i^2 = constant$ is a common finding for competing orders, but in Eq. 9 the meaning of Δ_0 is unknown, and the right-hand side is not constant, but vanishes when the VHS is at the Fermi level. This is suggestive of yet another quantum critical point (QCP) in the cuprates, but this one associated with the VHS.[3,54] Unlike most VHS-related features, in this case the gap scales to zero at the VHS, suggestive of nesting of the antinodal parts of the Fermi surface.[54]

Remarkably, QCPs have been proposed at three dopings in the cuprates: in the underdoped regime, where superconductivity is lost in a superconductor-insulator transition, near optimal doping, and now in the overdoped regime, where superconductivity vanishes near a VHS. Equation 9, or its generalization to multiple order parameters, offers a rationale for such a series of transitions, as the shrinking nesting inaugurates an ever more desparate competition among phases.

IV. DISCUSSION

The present calculations strongly support the idea that a competing order pseudogap provides a good description of two gap physics in hole doped cuprates.[9,53] The model offers new insights into the role of the VHS. It has been widely debated whether tunneling measurements can see the VHS[7,8]. The results are quite revealing and show that over the entire doping range studied, the feature conventionally identified as the VHS (orange dotted line in Fig. 4) is actually a gap feature[3,55] which can be traced to the bottom of the upper magnetic band. This explains why no VHS is found in normal state tunneling near optimal doping when the superconductivity is turned off. The calculation also provides insight into the transition to a large-gap insulator at half filling. The AF pseudogap is essentially given by the separation between the VHS and the bottom of the upper magnetic band, features A and B in Figs. 2(b), 2(c). From Fig. 2(a), this can be seen to be approximately 0.3 eV at $x = 0.08$, and the route to a 2 eV gap at half filling is clear.

Instead, we find the true VHS feature at higher energies. The doping evolution is consistent with that found in overdoped Bi2201 cuprate[8] where the VHS is clearly seen close to the Fermi level. The anticorrelation of the VHS peak with superconductivity could arise because the VHS can drive a competing ferromagnetic instability.[39,56]

It should be noted that the present model is not consistent with the conventional picture of peak-dip-hump[6].

By a relatively small change of parameters we have found a second solution, much closer to this conventional form. While this model reproduced many of the features of the STM data, it was ultimately less satisfactory than the model described in the text. In Appendix C, we briefly review this peak-dip-hump model. Among other problems noted in Appendix C, the peak-dip-hump model is unable to explain the transition to a large-gap insulator at half filling, producing a magnetic gap of only ∼100 meV even at the lowest doping.

While cuprates have traditionally been treated in strong coupling formalism, recent investigations have shown that intermediate coupling models, such as the present QP-GW model, can capture many salient features of cuprate physics, including the doping dependence of dispersion and optical properties[57–60]. In particular, our QP-GW self-energy successfully describes the dressing of low-energy quasiparticles by spin and charge fluctuations,[60] the high-energy kink (HEK) seen in ARPES,[60] the residual Mott bands in the optical spectra,[59] gossamer features,[61] anomalous spectral weight transfer with doping[62], and the magnetic resonance in neutron scattering.[63] In fact, our intermediate coupling model yields a number of characteristic signatures of strong coupling physics of the Hubbard model, including suppression of double occupancy[64], the $t-J$-model dispersions[65], spin wave dispersion[66], the $1/U$ scaling of the magnetic order,[67] and the phenomenon of anomalous spectral weight transfer (ASWT)[62,68,69]. Interestingly, a recent variational calculation finds a smooth evolution from a SDW to a Mott gap with increasing U, with no intervening phase transition or spin liquid phase in the cuprate parameter range.[70]

V. SUMMARY AND CONCLUSIONS

We have carried out a realistic, multiband modeling of STS spectra in Bi2212 over a wide doping range where effects of competing pseudogap and superconducting gaps are incorporated, and strong electron correlations are treated by introducing self-energy corrections in the one-particle propagators. The theoretical spectra capture many of the salient features of the corresponding experimental spectra and their doping dependencies, including the two-gap behavior at low energies, electron-hole asymmetry of the coherence peaks, and the presence of a prominent hump feature at high energies. Our analysis yields insight into the complex manner in which the VHS manifests itself in the STS spectra.

Acknowledgments It is a pleasure to acknowledge technical assistance of Mr. Ray Wang. This work is supported by the US Department of Energy, Office of Science, Basic Energy Sciences contract DE-FG02-07ER46352, and benefited from the allocation of supercomputer time at NERSC, Northeastern University's Advanced Scientific Computation Center (ASCC) and the resources of Institute of Advanced Computing, Tampere. I.S would like to thank Ulla Tuominen Foundation for financial support.

Appendix A: Details of interaction terms in the Hamiltonian

Here we provide details concerning the superconducting and antiferromagnetic terms in Eq. 7. The mean field superconducting coupling between electrons and holes is of the form

$$\Delta_{\alpha\beta} = \sum_{ab} U_{\alpha\beta ab}\langle c_{a\downarrow} c_{b\uparrow}\rangle. \tag{A1}$$

We assume a d-wave form for the gap as is appropriate in the cuprates.[10] The interaction $U_{\alpha\beta ab}$ is not known, and hence we follow the common practice of introducing a gap parameter, which gives the correct gap width and symmetry[71]. The gap values of $|\Delta| = 25 - 45meV$, plotted as violet squares in Fig, 4, are chosen to model the experimental spectra[17,29]. It is interesting to note that the gap calculated from a spin fluctuation mechanism[39] (red circles in Fig. 4) has a very similar doping dependece, andeed a very similar magnitude to the smaller gap feature.

Based on the QP-GW results, we incorporate magnetic interactions into our model via an onsite interaction term

$$H^C = U_{\alpha\alpha} n_{\alpha\uparrow} n_{\alpha\downarrow} = U_{\alpha\alpha} c^\dagger_{\alpha\uparrow} c_{\alpha\uparrow} c^\dagger_{\alpha\downarrow} c_{\alpha\downarrow}. \tag{A2}$$

At mean field level, this reduces to a magnetic interaction

$$-\frac{1}{2} U_{\alpha\alpha}\langle m_\alpha\rangle \left(c^\dagger_{\alpha\uparrow} c_{\alpha\uparrow} - c^\dagger_{\alpha\downarrow} c_{\alpha\downarrow}\right),$$

where $m_\alpha = n_{\alpha\uparrow} - n_{\alpha\downarrow}$. In the present calculation, we assume a doping independent $U = 7.5\ eV$ and the $< m_\alpha >$ are found self-consistently from a mean field calculation.[29,44,72]

Appendix B: Details of Self-energy corrections

Details of the three contributions to the self-energy of Eq. 8 are as follows. In the phonon contribution Σ^L, the phonons are approximated by a Debye spectrum[73,74]. The self-energy can then be written as a convolution of the Debye spectrum with a constant density of states for the electrons as:[11]

$$\Sigma^L(\varepsilon) = -\frac{A}{\pi}\left((2z + i\pi) + \left(z^2 - 1\right)\ln\left(\frac{z-1}{z+1}\right)\right), \tag{B1}$$

where $z = (\varepsilon + i\eta)/(\hbar\Omega_d)$, $A = \frac{3\hbar}{4\Omega_d}\Gamma^2\rho$, and η is a convergence parameter. We assume the self-energy for simplicity to be of a diagonal form, and apply this to Cu-$d_{x^2-y^2}$ orbitals using $\hbar\Omega_d = 80meV$ and $A = 60meV$. When combined with Σ^H, these values yield a reasonable description of the peak-dip-hump structure and the smoothness of the spectrum.

For the electron-electron self-energy, Σ^H, we utilize a simple Fermi-liquid type self-energy[10], except for the antibonding CuO_2 band, nearest the Fermi level, for which we introduce a QP-GW self-energy,[59]

$$\Sigma^H(k,\omega) \;=\; \sum_q \int \frac{d\omega'}{2\pi} \Gamma G(k-q,\omega+\omega') W(q,\omega') \quad \text{(B2)}$$

where $W = (U^2/2) Im(3\chi_s + \chi_c)$ and U is appropriate to the one-band model. The RPA spin/charge susceptibilities are $\chi_{c/s}(q,\omega) = \chi_0(q,\omega)[1 \pm U\chi_0(q,\omega)]^{-1}$, and the bare two-particle correlation function $\chi_0(q,\omega)$ is the convolution of the green's function. Self-consistency in Σ is achieved by calculating an average renormalization factor $Z = (1 - d\Sigma/d\omega)^{-1}$ with the QP-GW method.[12,59–61]. The vertex correction is $\Gamma = 1/Z$.

For electron doped cuprates, the competing order is (π,π) antiferromagnetism, while the origin of the pseudogap is unclear in the hole-doped cuprates. We have shown[9] that the tunneling spectra are insensitive to the exact nature of the pseudogap, as long as it represents a density wave order [charge, spin, or flux phase] at (π,π), so here we model the pseudogap as a (π,π) AFM. Including a d-wave SC gap below T_c, the green's function becomes a $4 \times 4-$tensor. The QP-GW self-energies are calculated in a $(|k\rangle, |k+Q\rangle)$ basis, then transformed via a unitary transformation to a real-space basis involving the spin up and spin down sublattices. In this transformed self-energy matrix, the off diagonal terms are found to be small and of varying sign, and are neglected. The corresponding matrix elements for the spin up and spin down holes are obtained by using the relations derived in Ref. 11.

Finally, an impurity self energy $\Sigma^{imp}(\varepsilon) = -i5.0meV$ is used in the SC phase for all the orbitals, which produces a reasonable smearing in the low-energy region. For the normal state, a larger value of $\Sigma^{imp}(\varepsilon) = -i20.0meV$ is used to account for enhanced normal state broadening near the Fermi energy.

Appendix C: Peak-Dip-Hump Model

The calculations described in the main text involve a moderate band renormalization by correlation effects, corresponding to a renormalization factor $Z = 0.5$, similar to that found in LSCO and NCCO. However, in Bi2212 ARPES experiments suggested a much narrower coherent band, with $Z \sim 0.28$.[75] In this Appendix we briefly describe the results of a model calculation with this smaller Z value, which also reproduces many of the features of the data of Figs. 1-4.

This small-Z model reproduces a form of peak-dip-hump scenario. The strong renormalization means that the spectral weight below the Fermi level is split into a broad, weakly renormalized incoherent band (hump) and a narrow, strongly renormalized coherent band (peak). In this model, the broad feature at high energies, with the dispersion in Fig. 2, is the VHS of the incoherent band, while the coherent band has a VHS at much lower energies, which varies with doping exactly as the VHS derived from the ARPES dispersion[38,75], orange-dotted line in Fig. 4. When an AF pseudogap and d-wave superconductivity are included, this model also reproduces the two-gap physics of Fig. 4. The dip between these two VHS features closely follows the measured position of the magnetic resonance peak.[76].

There are several experimental features that this small-Z model does not successfully reproduce. For instance, the coherent VHS peak is always found to be more intense than the incoherent VHS, contrary to experiment, Fig. 3. This is not unexpected, as the QP-GW model is known to underestimate the incoherent spectral weight. However, there are additional problems, involving only the low energy, coherent spectral weight. Most importantly, there is a true, coherent VHS near the Fermi level, which should clearly appear as a low energy peak when the AF and superconducting orders are turned off, in sharp contradiction to the normal state results plotted in Fig. 1. A more subtle feature involves the electron-hole asymmetry of the larger of the two-gap features as a function of doping. In this doping range, the coherent VHS always lies below the Fermi level, so the negative energy peak should always be more intense, and indeed the peak asymmetry should increase with underdoping, as the VHS moves further from the Fermi level. However, at very low dopings, the experimental asymmetry reverses sign, Fig. 3(b). Indeed, this can be understood from the model calculations of Fig. 2(a). Feature B, the lower edge of the UMB, actually crosses the Fermi level, lying above it at low dopings. With this crossing, the theoretical asymetry reverses, in good agreement with experiment, Fig. 3(b). Finally, while the large-Z model clearly extrapolates to a large-gap insulator at half filling, the small-gap model does not. The magnetic gap is directly reflected in the two gap physics near the Fermi level. Hence, even at the lowest doping it remains of order $\sim$100 meV, and the manner in which a $\sim$2 eV gap arises at half filling remains a puzzle. It is for these reasons that we prefer the larger-Z model. The apparently accidental pinning of the bottom of the UMB near the Fermi level may actually be a signature of a cooperative interaction between the AF and superconducting order, thereby stabilizing both phases.

* Electronic address: jouko.nieminen@tut.fi

[1] J. Friedel, J. Phys. Cond. Matt. **1**, 7757 (1989); R.S. Markiewicz, J. Phys. Chem. Solids **58**, 1179 (1997).

[2] J.E. Hirsch and D.J. Scalapino, Phys. Rev. Lett. **56**, 2732 (1986).

[3] K.-S. Chen, S. Pathak, S.-X. Yang, S.-Q. Su, D. Galanakis, K. Mikelsons, M. Jarrell, and J. Moreno, Phys. Rev. B**84**, 245107 (2011).

[4] A. Ino, C. Kim, M. Nakamura, T. Yoshida, T. Mizokawa, A. Fujimori, Z.-X. Shen, T. Kakeshita, H. Eisaki, and S. Uchida, Phys. Rev. B**65**, 094504 (2002).

[5] A. Kaminski, S. Rosenkranz, H.M. Fretwell, M.R. Norman, M. Randeria, J.C. Campuzano, J-M. Park, Z.Z. Li, and H. Raffy, Phys. Rev. B**73**, 174511 (2006).

[6] M.R. Norman, H. Ding, J.C. Campuzano, T. Takeuchi, M. Randeria, T. Yokoya, T. Takahashi, T. Mochiku, K. Kadowaki, Phys Rev Lett **79**, 3506 (1997); Z.-X. Shen and J.R. Schrieffer, Phys. Rev. Lett. **78**, 1771 (1997); M. Eschrig, Adv. Phys. **55**, 47 (2006).

[7] G. Levy de Castro, Chr. Berthod, A. Piriou, E. Giannini, and Ø. Fischer, Phys. Rev. Lett. **101**, 267004 (2008); **105**, 099702 (2010); F. Onufrieva and P. Pfeuty, Phys. Rev. Lett. **105**, 099701 (2010).

[8] A. Piriou, N. Jenkins, C. Berthod, I. Maggio-Aprile, and Ø. Fischer, Nature Communications DOI:10.1038/ncomms1229.

[9] Tanmoy Das, R.S. Markiewicz, and A. Bansil, Phys. Rev. B**77**, 134516 (2008).

[10] J. Nieminen, H. Lin, R.S. Markiewicz, and A. Bansil, Phys. Rev. Lett. **102**, 037001 (2009).

[11] J. Nieminen, I. Suominen, R.S. Markiewicz, H. Lin, and A. Bansil, Phys. Rev. B**80**, 134509 (2009).

[12] S. Basak, Tanmoy Das, Hsin Lin, J. Nieminen, M. Lindroos, R.S. Markiewicz, and A. Bansil, Phys. Rev. B**80**, 214520 (2009).

[13] The one-band QP-GW model for the non-superconducting state has only one free parameter, which is the value of the Hubbard U at half filling, since the hopping parameters are taken from LDA and the doping dependence of U is calculated from screening by long-range Coulomb interactions.

[14] S. Zhou, H. Ding, and Z. Wang, Phys. Rev. Lett. **98**, 076401 (2007).

[15] W.D. Wise, K. Chatterjee, M.C. Boyer, T. Kondo, T. Takeuchi, H. Ikuta, Z. Xu, J. Wen, G.D. Gu, Y. Wang, and E.W. Hudson, arXiv:0811.1585.

[16] This assumption has however been questioned[17,18].

[17] K. McElroy, Jinho Lee, J.A. Slezak, D.-H. Lee, H. Eisaki, S. Uchida, and J.C. Davis, Science **309**, 1048 (2005).

[18] T.S. Nunner, B. M. Andersen, A. Melikyan, and P.J. Hirschfeld, Phys. Rev. Lett. **95**, 177003 (2005).

[19] A.L. Fetter and J.D. Walecka, *Quantum Theory of Many-Particle Systems.* Dover (2003).

[20] Spin-flip terms are neglected in the present calculations.

[21] T.N. Todorov, G.A.D. Briggs and A.P. Sutton, *J.Phys.: Condens. Matter* **5**, 2389 (1993); J.B. Pendry, A.B. Prêtre and B.C.H. Krutzen, ibid., **3**, 4313 (1991).

[22] J. Tersoff and D.R. Hamann, *Phys. Rev. B* **31**, 805 (1985).

[23] I. Martin, A.V. Balatsky, and J. Zaanen, *Phys. Rev. Lett.* **88**, 097003 (2002).

[24] For present purposes, only short-range magnetic order is needed, as reported in M. Le Tacon, G. Ghiringhelli, J. Chaloupka, M. Moretti Sala, V. Hinkov, M.W. Haverkort, M. Minola, M. Bakr, K.J. Zhou, S. Blanco-Canosa, C. Monney, Y.T. Song, G.L. Sun, C.T. Lin, G.M. De Luca, M. Salluzzo, G. Khaliullin, T. Schmitt, L. Braicovich, and B. Keimer, Nature Physics **7**, 725 (2011).

[25] The doping dependence of the band structure is treated within the framework of the rigid band model [Ref. 26], which is expected to be a good approximation for doping away from the CuO_2 planes. It will be interesting to further examine doping effects by using first principles approaches[27].

[26] A. Bansil, Zeits. für Natur. **48** A, 165 (1993); Hsin Lin, S. Sahrakorpi, R.S. Markiewicz, and A. Bansil, Phys. Rev. Lett. **96**, 097001 (2006); H. Asonen, M. Lindroos, M. Pessa, R. Prasad, R.S. Rao, and A. Bansil, Phys. Rev. B **25**, 7075 (1982).

[27] L. Schwartz and A. Bansil, Phys. Rev. B **10**, 3261(1974); R. Prasad and A. Bansil, Phys. Rev. B21, 496 (1980); S.N. Khanna, A.K. Ibrahim, S.W. McKnight, and A. Bansil, Solid State Commun. **55**, 223 (1985).

[28] A.N. Pasupathy, A. Pushp, K.K. Gomes, C.V. Parker, J. Wen, Z. Xu, G. Gu, S. Ono, Y. Ando, and A. Yazdani, Science **320**, 196 (2008).

[29] The gap values are $\Delta = (25, 35, 35, 45, 45)$ meV and the magnetization values m are $= (0, 0.04, 0.08, 0.12, 0.16)$, for $x =$ (0.19,0.16,0.12,0.10,0.08).

[30] M. J. Lawler, K. Fujita, Jhinhwan Lee, A. R. Schmidt, Y. Kohsaka, Chung Koo Kim, H. Eisaki, S. Uchida, J. C. Davis, J. P. Sethna, and Eun-Ah Kim Nature 466, 374 (2010).

[31] Comparing Figs. 1 and 2 at high positive energies, the experimental spectra are seen to be quite different. Such an effect is neither expected nor seen in the theoretical spectra. The origin of this sample dependence of the spectra is not clear.

[32] I.M. Vishik, W.S. Lee, R.-H. He, M. Hashimoto, Z. Hussain, T.P. Devereaux, and Z.-X. Shen, New Journal of Physics **12**, 105008 (2010).

[33] K. McElroy, R.W. Simmonds, J.E. Hoffman, D.-H. Lee, J. Orenstein, H. Eisaki, S. Uchida, and J.C. Davis, Nature **422**, 592 (2003).

[34] W.S. Lee, I.M. Vishik, K. Tanaka, D.H. Lu, T. Sasagawa, N. Nagaosa, T.P. Devereaux, Z. Hussain, and Z.-X. Shen, Nature (London) **450**, 81 (2007).

[35] K. Tanaka, W.S. Lee, D.H. Lu, A. Fujimori, T. Fujii, Risdiana, I. Terasaki, D.J. Scalapino, T.P. Devereaux, Z. Hussain, and Z.-X. Shen, Science **314**, 1910 (2006).

[36] M. Le Tacon, A. Sacuto, A. Georges, G. Kotliar, Y. Gallais, D. Colson, and A. Forget, Nat. Phys. **2**, 537 (2006).

[37] W. Guyard, M. Le Tacon, M. Cazayous, A. Sacuto, A. Georges, D. Colson, and A. Forget, Phys. Rev. B**77**, 024524 (2008).

[38] M.R. Norman, M. Randeria, H. Ding, and J.C. Campuzano, Phys. Rev. B**52**, 615 (1995). This calculation neglects bilayer splitting.

[39] R. S. Markiewicz and A. Bansil, Phys. Rev. B **78**, 134513 (2008).

[40] When the imaginary part of the self-energy is non-zero, the Green's function no longer possesses real poles, and strictly speaking, we cannot think in terms of the usual energy bands. It can be useful however to think in terms

of complex energy bands defined by the complex energy solutions of $G(E,k)^{-1}=0$ as a function of k. See, Ref. 41

[41] A. Bansil, Phys. Rev. B **20**, 4025 (1979); A. Bansil, Phys. Rev. B **20**, 4035(1979); L. Huisman, D. Nicholson, L. Schwartz and A. Bansil, Phys. Rev. B 24, 1824 (1981).

[42] We should keep in mind that the tunneling matrix element plays a substantial role in modulating the LDOS to yield the STS spectra. Such matrix element effects are important in ARPES[43], inelastic light scattering[27,44,45] and other spectroscopies[46].

[43] M. C. Asensio, J. Avila, L. Roca, A. Tejeda, G.D. Gu, M. Lindroos, R.S. Markiewicz, and A. Bansil, Phys. Rev. B **67**, 014519(2003); A. Bansil, M. Lindroos, S. Sahrakorpi, and R.S. Markiewicz, Phys. Rev. B **71**, 012503 (2005); M. Lindroos and A. Bansil, Phys. Rev. Lett. **77**, 2985 (1996).

[44] R. S. Markiewicz and A. Bansil, Phys. Rev. Lett. **96**, 107005 (2006); Y. W. Li, D. Qian, L. Wray, D. Hsieh, Y. Xia, Y. Kaga, T. Sasagawa, H. Takagi, R.S. Markiewicz, A. Bansil, H. Eisaki, S. Uchida, and M.Z. Hasan, Phys. Rev. B **78**, 073104 (2008).

[45] G. Stutz, F. Wohlert, A. Kaprolat, W. Schülke, Y. Sakurai, Y. Tanaka, M. Ito, H. Kawata, N. Shiotani, S. Kaprzyk, and A. Bansil, Phys. Rev. B **60**, 7099 (1999); P. E. Mijnarends and A. Bansil, Phys. Rev. B **13**, 2381 (1976).

[46] L. C. Smedskjaer, A. Bansil, U. Welp, Y. Fang, and K.G. Bailey, J. Phys. Chem. Solids **52**, 1541(1991); J. C. Campuzano, L.C. Smedskjaer, R. Benedek, G. Jennings, and A. Bansil, Phys. Rev. B **43**, 2788 (1991); J. Mader, S. Berko, H. Krakauer and A. Bansil, Phys. Rev. Letters 37, 1232(1976).

[47] Y. Kohsaka, C. Taylor, P. Wahl, A. Schmidt, J. Lee, K. Fujita, J. W. Alldredge, Jinho Lee, K. McElroy, H. Eisaki, S. Uchida, D.-H. Lee, and J. C. Davis, Nature **454**, 1072 (2008).

[48] A. Pushp, C.V. Parker, A.N. Pasupathy, K.K. Gomes, S. Ono, J. Wen, Z. Xu, G. Gu, and A. Yazdani, Science **324**, 1689 (2009).

[49] S. Huefner, M.A. Hossain, A. Damascelli, and G.A. Sawatzky, Rep. Prog. Phys. **71**, 062501 (2008).

[50] J.E. Hirsch, Phys. Rev. B**59**, 11962 (1999).

[51] These are matrix elements of the Green function between majority/minority spin electrons at a chosen site and the holes with the opposite spin at a neighbouring site ($F_{\alpha\beta maj}=\langle e_{\alpha\sigma(maj)}|\mathbf{G}|h_{\beta-\sigma(maj)}\rangle$ and $F_{\alpha\beta min}=\langle e_{\alpha\sigma(min)}|\mathbf{G}|h_{\beta-\sigma(min)}\rangle$). Their imaginary part measures the pairing amplitudes of electrons with opposite spins.

[52] G. Bilbro and W.L. McMillan, Phys. Rev. B**14**, 1887 (1976).

[53] While we have modeled the pseudogap as due to AFM order, any other competing (π,π) density-wave order would work equally well[9].

[54] R.S. Markiewicz, J. Lorenzana, G. Seibold, and A. Bansil, Phys. Rev. B**81**, 014509 (2010).

[55] See Fig. 17 of R.S. Markiewicz, Phys. Rev. B**70**, 174518 (2004).

[56] J.G. Storey, J.L. Tallon, and G.V.M. Williams, Phys. Rev. B**76**, 174522 (2007).

[57] A. Comanac, L de Medici, M. Capone, and A. J. Millis, Nature Physics, **4** 287 (2008); L. de' Medici, X. Wang, M. Capone, and A.J. Millis, Phys. Rev. B **80**, 054501 (2009).

[58] C. Weber, K. Haule, and G. Kotliar, Nat. Phys. **6**, 574 (2010).

[59] T. Das, R.S. Markiewicz, and A. Bansil, Phys. Rev. B **81**, 174504 (2010).

[60] R.S. Markiewicz, S. Sahrakorpi, and A. Bansil, Phys. Rev. B **76**, 174514 (2007).

[61] T. Das, R.S. Markiewicz, and A. Bansil, Phys. Rev. B **81**, 184515 (2010).

[62] R.S. Markiewicz, T. Das, and A. Bansil, Phys. Rev. B**82**, 224501 (2010).

[63] A. Bansil, Susmita Basak, Tanmoy Das, Hsin Lin, M. Lindroos, J. Nieminen, Ilpo Suominen, and R.S. Markiewicz, J. Phys. Chem. Solids **72**, 341 (2011).

[64] The mean-field AFM suppresses double occupancy so well that Gutzwiller projection on an AFM ground state actually *increases* double occupancy. See P. Fazekas, "Lecture Notes on Electron Correlation and Magnetism", (World Scientific, Singapore, 1999).

[65] Even at mean-field level, the large-U limit antiferromagnet reproduces the one-hole [electron] dispersion of the lower [upper] Hubbard band in the $t-J$ model. Self energy corrections add an incoherent part to the dispersion (t-scale).

[66] J. R. Schrieffer, X. G. Wen, and S. C. Zhang, Phys. Rev. B**39**, 11663 (1989).

[67] A characteristic feature of Mott physics is that as U increases the Mott gap grows but the magnetic transition temperature ultimately decreases. This follows in the present formalism: even though the gap grows, the energy difference between any two magnetically ordered phases scales with $J\sim 1/U$.

[68] Doping a Mott insulator leads to anomalous spectral weight transfer (ASWT): removing one electron from a Mott insulator leads to two empty states at low energies (in the lower Hubbard band), since there is no longer a penalty U to be paid when the spin-reversed electron occupies the state[69]. The QP-GW model captures most of this effect, due to the real collapse of the magnetic gap at a quantum critical point.[62] QP-GW underestimates this ASWT in the very low doping regime, although here strong disorder may mask this effect, and render it unobservable.

[69] H. Eskes, M.B. Meinders, and G.A. Sawatzky, Phys. Rev. Lett. **67**, 1035 (1991).

[70] L.F. Tocchio, F. Becca, A. Parola, and S. Sorella, Phys. Rev. B**78**, 041101(R) (2008).

[71] J.-M. Tang and M. E. Flatté, Phys. Rev. **B 66**, 060504(R) (2002); J.-M. Tang and M. E. Flatté, Phys. Rev. **B 70**, 140510(R) (2004).

[72] H. Lin, R.S. Markiewicz, and A. Bansil, unpublished.

[73] W.E. Pickett, Rev. Mod. Phys. **61**, 433(1989).

[74] R.E. Cohen, W.E. Pickett, and H. Krakauer, Phys. Rev. Lett. **62**, 831(1989).

[75] R.S. Markiewicz, S. Sahrakorpi, M. Lindroos, Hsin Lin, and A. Bansil, Phys. Rev. B**72**, 054519 (2005).

[76] J.F. Zasadzinski, L. Ozyuzer, N. Miyakawa, K.E. Gray, D.G. Hinks, and C. Kendziora, Phys. Rev. Lett. **87**, 067005 (2001).